Thrust Vector Control by Liquid Injection into Rocket Nozzles

ROBERT SEHGAL* AND JAIN-MING WU†
Jet Propulsion Laboratory, California Institute of Technology, Pasadena, Calif.

An analytical model is constructed to represent the interaction between the injected liquid and the supersonic stream by considering the mechanism of atomization, the rate of evaporation, and the motion of droplets, based on the injectant and gas properties. The body shape because of the generated vapor is calculated from basic drag equations; then the flow interference pattern, including the shock waves owing to turbulent boundary-layer separation, is investigated. The total side force is computed by summing the reaction force due to the liquid jet, the force due to the excess pressure on the nozzle wall downstream of the shock pattern, and the contribution due to the separated region. Numerical examples are presented for two cases, results of which compare favorably with available test data.

Nomenclature

A = cross-sectional area, ft²
$C_{P\,g-v}$ = average specific heat at constant pressure of gas-vapor mixture
C_{Pv} = average specific heat at constant pressure of vapor over temperature range $T_0 - T_l$
d = droplet diameter at any time t, ft
d_i = injector port diameter, ft
d_0 = mean droplet diameter at injection, ft
d_{30} = volume-median droplet diameter, ft
D = drag in Eq. (3), lbf
h = liquid heat of vaporization corresponding to p_w, Btu/(lb-mole)
k = gas thermal conductivity, Btu/ft-sec°R
k_{g-v} = average heat conductivity of gas-vapor mixture
$\dot{m}$ = mass flow rate, slug/sec
M_0 = freestream Mach number
$\mathfrak{M}$ = molecular weight
p_c = chamber pressure, psi
P = static pressure, psi
P_t = total pressure, psi
Q = volume flow rate, ft³/sec
r = radius of droplet at any time t, ft
r_0 = radius of droplet at injection, ft
Re = Reynolds number, $dV\rho/\mu$
t = time, sec
T = temperature, °R
V = velocity, fps
$\dot{W}$ = weight flow rate, lb/sec
We = Weber number, $\sigma_l/\rho V^2 d_0$
α = cone half-angle
β = $(M^2 - 1)^{1/2}$
γ = ratio of specific heats of gas
δ_f = deflection angle, deg
δ_s = separation angle, deg
ϵ = nozzle expansion ratio
ζ = injection angle, deg
θ = shock-wave angle, deg
λ = evaporation rate, ft²/sec
μ = Mach wave angle, $\sin^{-1} M^{-1}$
μ_g = gas viscosity, lbf-sec/ft²
μ_l = liquid viscosity
ν = gas kinematic viscosity, ft²/sec; also Prandtl-Meyer angle
ξ = density ratio across shock $[(\gamma - 1)M_0^2 + 2]/(\gamma + 1)M_0^2$
ρ = density, lb/ft³
σ_l = liquid surface tension

Subscripts

d = droplet
g = gas
i = injector, injectant
l = liquid
L = laminar flow
0 = freestream properties at point of injection
T = turbulent flow
v = vapor
w = wall

Received September 4, 1963; revision received April 24, 1964. This paper presents the results of one phase of research carried out at the Jet Propulsion Laboratory, California Institute of Technology, under Contract NAS 7-100, sponsored by NASA.

* Engineering Specialist. Associate Fellow Member AIAA.
† Graduate Student, California Institute of Technology. Member AIAA.

Introduction

THE practical aspects of changing the thrust direction of a rocket motor by liquid injection into the supersonic stream of the rocket exhaust are well established by numerous experimental data; however, the complex interaction between the secondary injectant and the primary flow is not well understood and is not readily amenable to theoretical analysis. Many approximate analytical solutions for predicting the induced side force have been generated, and a complete review is available.[1] Most of the published work is concerned with gaseous injection, and relatively little work has been devoted to the analytical study of liquid injection, because atomization, evaporation, jet penetration, and mixing are difficult to analyze. Moreover, a liquid with a high vapor pressure (relative to exhaust stream pressure), such as Freon 12, will flash vaporize. There is no work available on atomization with flash evaporation, and it is doubtful that any available work on atomization would yield reasonable results when applied to a system undergoing flash evaporation.

Wu et al.[2] presented a simple analytical model for calculating the side force generated by liquid injection, but the physical nature of atomization and evaporation was ignored. Recent work of Wu et al.[3] shows a process for calculating the displacement body shape based on oversimplified assumptions, such as 1) the droplet Reynolds numbers are so small that Stokes flow exists throughout the region of vaporization, and 2) the vaporization rate is constant throughout the region of vaporization. Also, the formulated model for the flow interference did not agree with the shock patterns visualized from schlieren photographs and spark shadowgraphs obtained from tests conducted at the Jet Propulsion Laboratory.

Recognizing these inadequacies, it is the objective of this paper to develop an improved analytical model for liquid injection. A general schematic of secondary fluid injection into the rocket nozzle exhaust is shown in Fig. 1. The in-

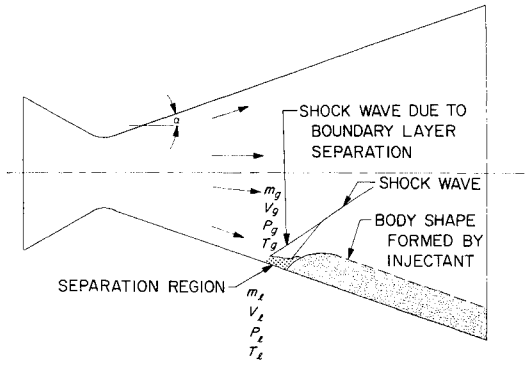

Fig. 1 Schematic of secondary fluid injection.

jectant liquid creates a disturbance, and the pressure field created on the wall causes the side force. The resultant total side force can be expressed as

$$F_t = F_1 + F_2 + F_3 \tag{1}$$

where F_1, F_2, and F_3 are the side-force contributions owing to the momentum of the liquid, the separated region ahead of the injector, and the pressure disturbance downstream of the injector, respectively. The injectant liquid considered in this study, Freon 113, is one which has a low vapor pressure relative to the pressure it encounters during the injection process, thus eliminating the phenomenon of flash evaporation.

Analysis

The liquid jet, with velocity V_i, penetrates the supersonic gas stream and breaks up into small spherical droplets,

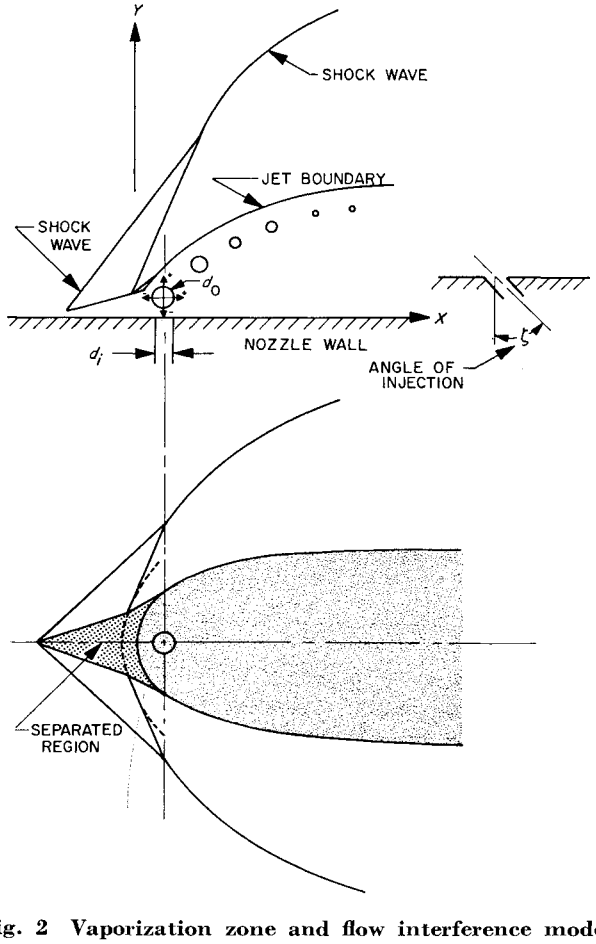

Fig. 2 Vaporization zone and flow interference model.

which evaporate as they are carried downstream. The equation describing the motion of a spherical droplet is

$$ma = D = C_D A_d \rho_g V_r^2/2 \tag{2}$$

where V_r is the relative velocity between the exhaust gas and the droplet. For simplicity, the nozzle wall is treated as a flat plate extended to the exit, and the nozzle axis is in the horizontal direction. The summations of forces on an evaporating droplet (Fig. 2) are

$$\tfrac{4}{3}\pi r^3 \rho_l a_x = \tfrac{1}{2}\rho_g C_D A_d (V_g - V_x)^2 + g m_d \sin\alpha \tag{3}$$

$$-\tfrac{4}{3}\pi r^3 \rho_l a_y = \tfrac{1}{2}\rho_g C_D A_d (V_y)^2 + g m_d \cos\alpha \tag{4}$$

Simplifying Eqs. (3) and (4) and solving them for the accelerations gives

$$a_x = C_1 + 0.375 C_{Dx}(V_g - V_x)^2 \dot{m}_g V_i A_i / r \dot{m}_l V_g A_g \tag{5}$$

$$-a_y = C_2 + 0.375 C_{Dy} V_y^2 \dot{m}_g V_i A_i / r \dot{m}_l V_g A_g \tag{6}$$

where C_1 and C_2 are gravitational constants that depend upon the nozzle half-angle, $C_1 \equiv g \sin\alpha$ and $C_2 \equiv g\cos\alpha$, and the initial values (at $t = 0$) of V_x and V_y depend on the injection angle ζ, $V_x = -V_i \sin\zeta$ and $V_y = V_i \cos\zeta$. For the solution of the foregoing equations, the size of the liquid droplet and its evaporation rate and drag coefficients, which are functions of the droplet Reynolds number, must be known at any time t.

Atomization

Atomization as implied here refers to the process of breaking the mass of liquid injectant into small droplets when the liquid jet encounters the high-velocity gas stream. A successful analysis should result in expressions describing the size distribution of drops as a function of liquid physical properties, geometry of the system, and operating conditions. Unfortunately, such complete theoretical derivations are not available, but several empirical relationships are available. Two such derivations of significant interest which show mean drop-size derivations are the empirical relationships of Ingebo and Foster[4] and Nukiyama-Tanasawa.[5] In both of these relationships, which agree favorably with their respective experimental data, some important physical parameters seem to have been ignored.

Ingebo and Foster[4] measured drop-size distribution for liquid jets atomized by cross-stream injection into subsonic air streams and developed the following empirical relationship for the mean droplet diameter:

$$d_{30} = 3.9 d_i (We/Re)^{0.25} \tag{7}$$

Substituting for the Weber and Reynolds numbers and rewriting gives

$$d_0 = 3.9(0.0328)(\sigma_l \mu_l / \rho_g \rho_l V_g^3)^{0.25} d_i^{0.5} \tag{8}$$

This relationship shows a dependence of the initial drop mean diameter on the injector diameter but ignores any dependence on the liquid or gas flow rate.

The empirical relationship developed by Nukiyama-Tanasawa[5] is described as follows:

$$d_0 = \frac{5.85}{V_g}\left(\frac{\sigma_l}{\rho_l}\right)^{0.5} + 0.0579\left(\frac{\mu_l}{(\sigma_l \rho_l)^{1/2}}\right)^{0.45}\left(\frac{1000 Q_l}{Q_g}\right)^{1.5} \tag{9}$$

This derivation is dimensionally inconsistent but seems to agree favorably with data in the literature. The relationship shows a dependence on the volumetric flow rates of liquid and gas but shows no dependence on the gas density or injector diameter. Bitron[6] has shown a reasonably good agreement of this relationship with experimental data when $Q_l \approx Q_g$ at low supersonic conditions. However, in the case of liquid-injection thrust vector control, Q_l is significantly smaller than Q_g, and it seems that in the Nukiyama-Tanasawa

relationship, Q_g should be modified for the local region near the injector, because injection is a local phenomenon.

Since no better correlation based on data for supersonic gas-flow conditions is available, the one by Ingebo and Foster is used in the present work. Mean droplet diameter is computed for two sets of gas conditions: 1) flow behind a normal shock, and 2) freestream conditions. The first case gives a larger initial mean droplet diameter, but the computed particle trajectories are essentially the same for both cases, because of the greater evaporation rate in the first case.

Evaporation

For liquid-injection thrust vector control, liquid vaporization is of significant importance in maintaining excess pressure downstream of the injector. Once the initial mean droplet diameter is known, the next quantity to be determined is the rate of droplet vaporization. The droplet mass and volume should be continuously diminishing as it travels downstream of the nozzle, owing to evaporation. According to Godsave's derivation,[7] the instantaneous droplet diameter is related to the initial diameter by the relationship

$$d^2 = d_0^2 - \lambda t \tag{10}$$

where λ is the evaporation rate (ft^2/sec). For laminar flow, Godsave[8] has experimentally determined the relationship

$$\lambda_L = (8K_{g-g}/\rho_l C_{Pg-v}) \ln[1 + C_{Pv}(T_g - T_l)/h] \tag{11}$$

Agoston et al.[9] modified this evaporation rate for the turbulent flow case in terms of the droplet Reynolds number and Prandtl number by the following expression:

$$\lambda_T = \lambda_L(1 + 0.276Re^{1/2}Pr^{1/3}) \tag{12}$$

Droplet Drag Coefficient

In order to determine the body shape or the trajectory of a droplet, the drag coefficient[10] of the droplet at any time t must be known. The basic equation of drag coefficient can be written as

$$C_{D_{x,y}} = \frac{C_{D_{0x,y}}}{K_M{}^2} f(M) \times$$

$$\begin{cases} f(M) = 1 & \text{for} \quad 0 < M < 0.5 \\ f(M) = 0.689(M + 0.952) & \text{for} \quad 0.5 < M < 2 \end{cases} \tag{13}$$

where M is the relative Mach number. The values of $C_{D_{0x,y}}$ can be determined by using Stokes' law and the least squares fit of drag data[11] as presented by Stonecypher[12]:

$$C_{D_{0x,y}} = 24/Re \qquad \text{for} \qquad 0 < Re < 0.1 \tag{14}$$

and

$$\ln C_{D_{0x,y}} = 3.27 - 0.889[\ln Re + 0.0342(\ln Re)^2 + 0.00144(\ln Re)^3] \qquad \text{for} \qquad 0.1 < Re < 1000$$

$$Re_x = d\rho_g(V_g - V_x)/\mu_g$$
$$Re_y = d\rho_g V_y/\mu_g \tag{15}$$

Droplet Trajectory and Gas-Body Shape

Once the initial droplet diameter is known, the droplet trajectory can be determined for variable mass, volume, and evaporation rate from Eqs. (5), (6), (10), and (13). The numerical example in Table 1 shows the trajectory calculations for two typical sets of experimental data.

The evaporation rates for laminar flow λ_L for the two cases were computed from Eq. (13) with the simplifying assumption that $k_{g-v}/C_{Pg-v} \cong \mu_g$.

Equations (5), (6), (10), (12), and (13) were programed on the IBM 7090 and droplet trajectories (Fig. 3) were computed for small time intervals. The computed trajectory for each case is for a typical droplet, and it is assumed that all of the droplets will follow this line trajectory, which can be thought of as representing a line source, generating vapor. Figure 3 indicates that the trajectories are very close to the wall; thus, it can be assumed that the generated body is a half-body of revolution, lying on the wall.

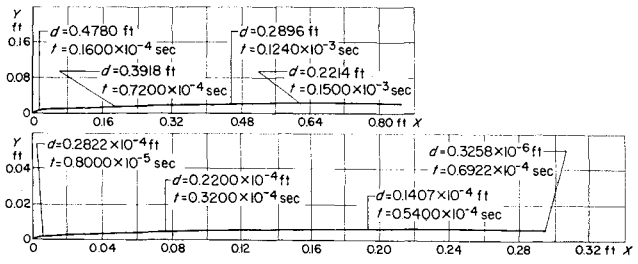

Fig. 3 Droplet trajectories (based on line source assumption) for cases 1 and 2 of Table 1.

The body shape because of generated vapor can be determined (cf. Ref. 13) by the following steps. From Eq. (10) we know that $d = d(t)$ or $d(x)$. Let $\dot{W}_{l_0}$ represent the total liquid-injection flow rate. Then the liquid flow rate at a distance x from the injection port can be expressed as

$$\dot{W}_l/\dot{W}_{l_0} = (1 - \lambda_T/d_0^2)^{3/2} \tag{16}$$

Thus the corresponding vaporized flow rate can be expressed as

$$\dot{W}_v = \dot{W}_{l_0} - \dot{W}_l = \dot{W}_{l_0}[1 - (1 - \lambda_T/d_0^2)^{3/2}] \tag{17}$$

This $\dot{W}_v(x)$ is produced by the line source or a typical droplet trajectory. Since the trajectories are so close to the wall (Fig. 3), we shall assume, for simplicity, that the area is a half-body of revolution and that its radius r_x can be calculated as a function of distance together with the trajectory

Table 1 Two typical operating cases for injection of Freon 113 (ζ = 0)

Parameter	Case 1	Case 2
Rocket chamber		
P_c, psi	410	365
$\dot{W}$, lb/sec	486	4.04
γ	1.20	1.25
$\mathfrak{M}_g$	25.0	23.5
T_t, °R	5226	5460
Mainstream at injection point		
$M_0 = M_g$	2.52	2.88
ρ_g, lb/ft^3	0.0157	0.0083
T_g, °R	3200	2740
V_g, fps	6955	7724
$P_0 = P_g$, psi, for		
λ = 1.25	21.45	10.28
λ = 1.2		9.75
$\mu_g \times 10^5$, lb/ft-sec	8.48	4.85
Nozzle and injectant		
ϵ at injection	3.5	5.16
α, deg	17	17.5
d_i, in.	0.345	0.110
V_l, fps	202	198
P_{t_l}, psi	1169	1114
W_l, lb/sec	13.1	1.1312
ρ_l, g/cc	1.6	1.6
μ_l, poises	0.0065	0.0065
σ_l, dynes/cm	18.5	18.5
T_l (boiling at P_w), °R	605	565
h, Btu/lb	≃45	≃45
$\bar{C}_{p_v}$, Btu/lb °R	≃0.55	≃0.55
$\mathfrak{M}_l$	187	187
$d_0 \times 10^{-6}$, ft; Eq. (8)	50	30
$\lambda_L \times 10^{-6}$, ft^2/sec; Eq. (11)	13.4	13.0

calculations. From the continuity equation and Eq. (17), we have

$$r_x = \left(\frac{2\dot{W}_v}{\pi\rho_v V_r}\right)^{1/2} = \left\{\frac{2\dot{W}_{l_0}}{\pi\rho_l V_c}\left[1 - \left(1 - \frac{\lambda_T}{d_0^2}\right)^{3/2}\right]^{1/2}\right\} \quad (18)$$

where the vapor density is defined by $\rho_v = \mathfrak{M}_v\rho_g/\mathfrak{M}_g$, and $\mathfrak{M}_v$ and $\mathfrak{M}_g$ are molecular weights of the vapor and the gas. Upon encountering high-temperature gas, the Freon 113 molecule splits in two. Thus an assumption is made in this analysis that the molecular weight of the vapor is approximately one-half the molecular weight of the injectant liquid.

Flow Interference Analysis

The next step required in the computation of the side force is the formulation of the flow interference model. For liquid injection, the flow interference models constructed to date do not agree with the shock patterns obtained from wind-tunnel tests at the Jet Propulsion Laboratory.[14]

Figure 4 shows schlieren and spark shadowgraph pictures for Freon 12 with an injection temperature of −75°F. The pictures show the shock patterns formed ahead of the injector owing to turbulent boundary-layer separation and the blunt-nose-shaped body owing to secondary flow. Figure 5 shows the shock patterns when Freon 12 is injected at approximately the same mass flow rate but at a temperature of +67°F. The higher-temperature run shows a larger separated region and a larger gas body blocking the main flow. From the spark shadowgraphs, which give instantaneous views of the process, it is seen that the body produced by the injectant at the higher injection temperature has a very ragged boundary, indicating that the jet is initially breaking up into large masses. This characteristic of Freon 12, the vapor pressure of which is higher than that of the Freon 113 used in the present study, at the higher injection temperature is attributed to flash vaporization.

In this study, as noted previously, the process of flash vaporization was not considered. The interference flow model developed is consistent with the shock patterns shown in Fig. 4 for the case where flash vaporization could not occur.

The detached bow shock wave caused by the blunt-nose-shaped body can be located with good accuracy by replacing the body by a sphere of the same radius, R_b (see Fig. 6). At $y = 0$, the standoff distance Δ_0 is

$$\Delta_0|_{y=0} = R_s - R_b \quad (19)$$

Now R_s (the curvature of the shock wave) and Δ_0 can be expressed in terms of R_b and the density ratio ξ by the foregoing relation and the constant density approximation theory,[15] as follows:

$$R_s = R_b f(\xi)/[1 - f(\xi)] \quad (20)$$

$$\Delta_0 = R_b\xi/[1 - f(\xi)] \quad (21)$$

where $f(\xi) \equiv 1 + (8\xi/3)^{1/2}$ and $\xi = [(\gamma - 1)M_0^2 + 2]/(\gamma + 1)M_0^2$.

In the usual supersonic flow region, it is a good approximation to use a hyperbolic equation to represent the bow shock wave. The asymptotes of this hyperbola are the freestream Mach waves. Therefore, by knowing the freestream conditions and R_s, one can determine the hyperbola (see Fig. 6):

$$y^2 = x^2/\beta^2 - \beta^2 R_s^2 \quad (22)$$

In Ref. 2 the shock wave caused by the boundary-layer separation was assumed to be a function of the freestream Mach number. This shock wave will either be a conical or a plane-oblique shock wave, depending on whether the injection port is a circular shape or a long slot. This shock wave will hit the bow shock wave ahead of the blunt-nose-shaped body.

In developing this analytical model, it was seen that the dividing stream line must make a turn near the nose of the

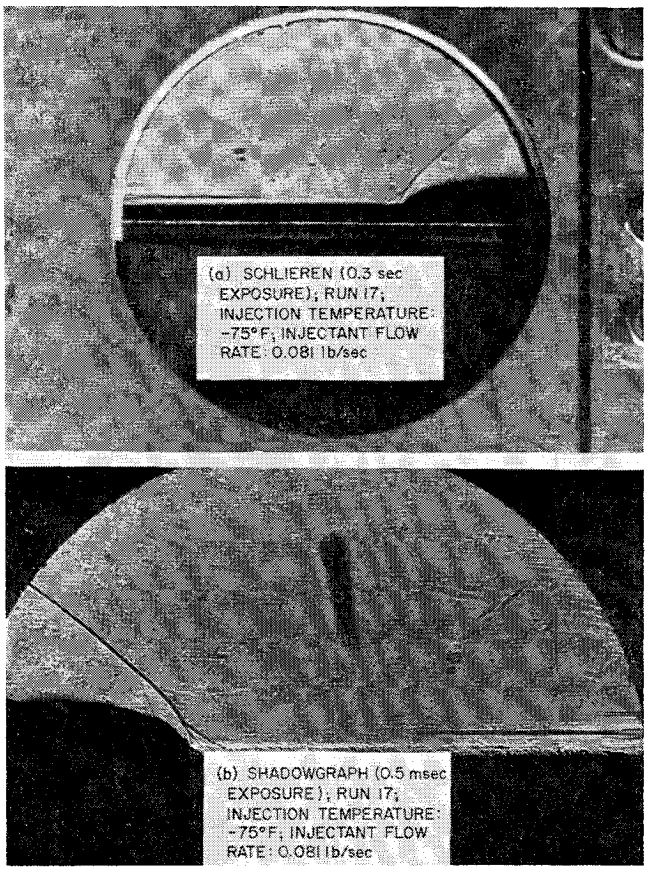

Fig. 4 Schlieren and spark shadowgraph for Freon 12 with an injection temperature of −75°F.

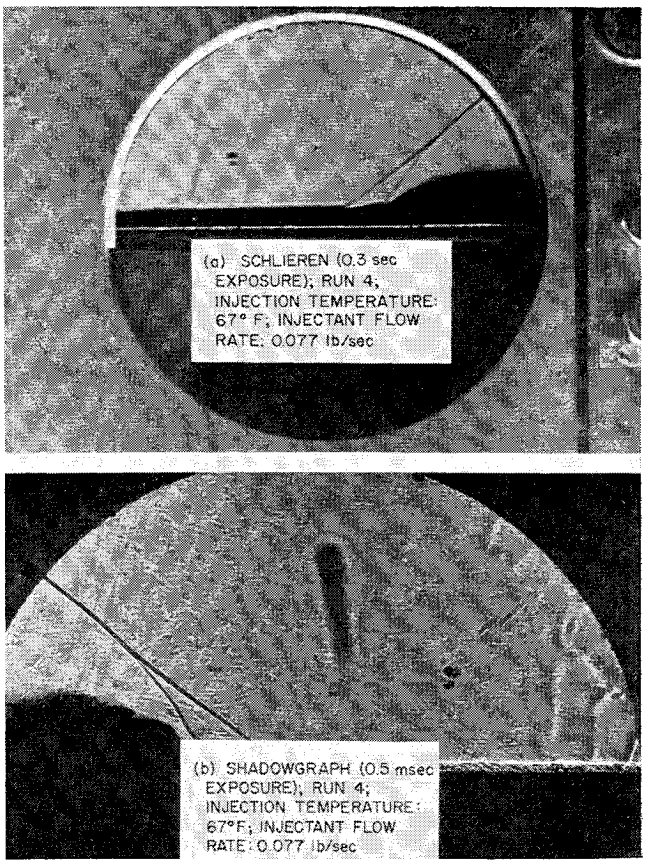

Fig. 5 Schlieren and spark shadowgraph for Freon 12 with an injection temperature of 67°F.

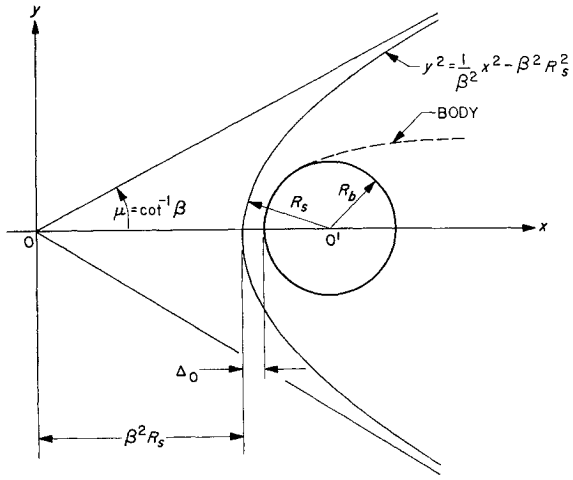

Fig. 6 Schematic of the bow shock wave created by a sphere R_b and its position.

blunt body. The consequence of this turn is an increase in the local separation region. The formation of a separation shock wave in this small local region is derived by considering the flow-turning phenomenon in Mager's analysis.[16] Therefore, the second shock wave owing to this local increase of the separation region can be determined by the conditions after the first shock wave. (In the conical separation case, use its average value.) The second shock is assumed to be approximately two-dimensional (a similar approach is indicated in Ref. 17), so that the second turning angle δ_{s2} can be determined from Fig. 7. Its corresponding shock-wave angle can be determined from Ref. 18. For simplicity, the stream line is approximated for this short distance by a straight line, which is to say that the dividing stream line will follow this turning angle. Let the stream line be tangent to the body, as shown in Fig. 8, and assume that this second turning will start on some point of the original bow shock wave. (This assumption is introduced because the initial turning is through this bow shock wave.) Thus one can determine the whole separation region and its introduced shock wave. The dividing stream line can pass through the body smoothly by making two turns. The original bow shock wave, owing to the existence of the body, will be expected to disappear because of the smooth flow. The second shock wave will go straight until it hits the first shock wave. There must exist some reflected wave to adjust the conditions at that particular point, but this reflection is considered weak and its effect is neglected in this analysis.

The body is approximated by several conical surfaces called, successively, regions 2, 3, . . . , etc., as shown in Fig.

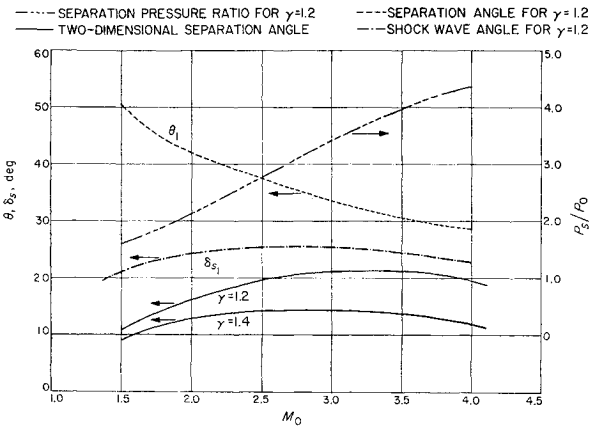

Fig. 7 Separation parameters vs freestream Mach number.

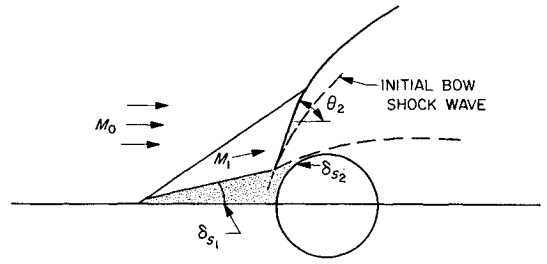

Fig. 8 Schematic of shock waves and the separation regions.

9. Downstream from region 2, an average shock-wave expansion is assumed by making use of the average Mach number determined in region 2. It is known that when the tangent to the body becomes flat (0° angle), the body static pressure will go back to the freestream condition. Thus the expansion process should satisfy this boundary condition. The several regions shown can be formed by calculating the Mach wave angle for each and assuming it is a straight line. Now the average pressure in each region can be calculated. The excess pressure over the freestream pressure multiplied by its corresponding area will represent the side-force contribution downstream of the shock waves.

Sample Calculations

The sample calculations[19] summarized in Table 2 for case 1 (Table 1) are made as follows (refer to Fig. 9): First the shock-wave pattern is determined. The expansion process starts from region 2; the initial flow-turning (expansion) angle $\Delta\delta$ is from 39.5° to 22°, which is equal to 17.5°. The average flow turning required to attain freestream static pressure is 37°. Thus the corrected value for satisfying the pressure which goes back to freestream value in region 6 is (17.5°) (37°)/39.5° = 16.4°.

The corresponding Prandtl-Meyer angle is found by adding $\Delta\delta$ to $\bar{\nu}$ for the previous region; thus $\bar{\nu}_3 = \bar{\nu}_2 + (\Delta\delta)_3 = 9.84 + 16.4 = 26.24°$.

The static wall pressure at the point of injection is $P_{w0} = 21.45$ psi. Since in this analysis average values are assumed, the Mach wave in each region can be represented by a straight line. Thus two straight lines have to be constructed from each point (*d*, *e*, *f*, and *g*) for $\bar{\mu}$ and for $\bar{\mu} + \delta$, where δ is measured from the horizontal.

The regions between each of the two lines are called regions 2–3, 3–4, 4–5, and 5–6, as shown in Fig. 9. The static pressure in each of these regions is assumed to be an average value from the neighboring regions. For case 1, the excess pressure for each region is $P - 21.45$ psi.

Calculation of Side Force

The side-force contribution owing to secondary momentum is

$$F_1 = (P_i - P_0)A_i + m_i V_i = 190 \text{ lb}$$

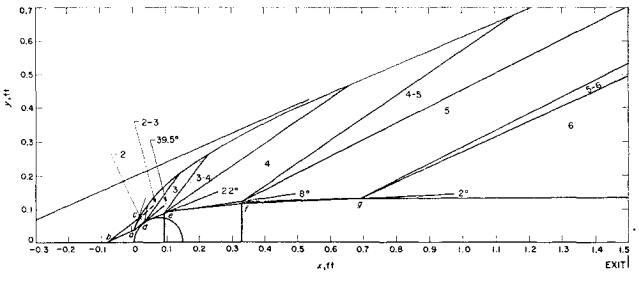

Fig. 9 Sample calculation of side force for case 1.

Table 2 Summary of interference flow field parameters used to compute side force for cases 1 and 2 of Table 1

Region	$\bar{M}$	$\Delta\delta$, deg	Corrected $\Delta\delta$, deg	$\bar{\nu}$, deg	P/P_{t_0}	P	δ	$\bar{\mu}$, deg	$\bar{\mu}+\delta$, deg	Area, in.^{2}	F_2+F_3, lbf
					Case 1						
1	1.825	...	...	...	0.178	73	...	...	...	0.36	14.7
2	1.39	...	...	9.84	0.307	126	37	46	83	0.38	39.5
2–3	...	...	...	...	...	93.6	...	...	...	0.41	29.2
3	1.86	17.5	16.4	26.24	0.149	61.2	20.6	32.5	53.1	1.73	69.2
3–4	...	...	...	...	...	46.8	...	...	...	3.92	102.0
4	2.23	14	13.1	39.34	0.0786	32.3	7.5	26.6	34.1	15.8	190.0
4–5	...	...	...	...	...	28.2	...	...	...	13.6	95.0
5	2.39	6	5.62	44.96	0.0588	24.1	1.88	24.7	26.85	31.0	80.5
5–6	...	...	...	...	...	22.8	...	...	...	2.7	3.5
6	2.45	2	1.88	46.84	0.0495	21.4	0	24	24	0	0
					Case 2						
1	2.135	...	...	...	0.09	32.8	...	...	...	0.023	0.50
2	1.61	...	...	17.48	0.204	74.5	39.6	38.3	77.9	0.072	4.66
2–3	...	...	...	...	...	51.8	...	...	...	0.115	4.83
3	2.17	21.5	20.0	37.48	0.080	29.2	19.6	27.4	46.9	0.18	2.72
3–4	...	...	...	...	...	23.1	...	...	...	0.49	6.03
4	2.47	11	10.2	47.68	0.0466	17.0	9.3	24	33.3	0.763	5.52
4–5	...	...	...	...	...	14.5	...	...	...	0.151	0.72
5	2.67	6.5	6.04	53.72	0.0328	12.0	3.3	22	25.3	0.98	2.2
					Nozzle exit						
5–6	...	...	...	...	...	11.18	...	...	...	...	...
6	2.74	2.5	2.32	55.98	0.0282	10.35	1	21.4	22.4	...	...
6–7	...	...	...	...	...	10.05	...	...	...	...	...
7	2.77	1	0.93	56.93	0.0267	9.75	0	21.2	21.2	...	...

The contribution to the side force (F_2 and F_3) from the individual regions is the excess pressure over the static free-stream pressure, times its area. This is shown by the last column of Table 2, which sums to 624 lbf. For the symmetrical body, the total normal side-force contribution owing to excess pressure is $2(F_2 + F_3) = 1248$ lbf; thus, from Eq. (1), $F_t = 1248 + 190 = 1438$ lbf.

The resultant computed side force (corrected perpendicular to center of nozzle axis) $= 1440 \times \cos 17° = 1380$ lbf. This is an exceptionally good agreement with the measured side force.

The foregoing procedure was also used to calculate the side force for case 2 (Table 1), as shown in the lower half of Table 2. The ratio of specific heats γ for this case is 1.25; however, $\gamma = 1.2$ was used to facilitate the computations. These calculations, shown in Table 2 and Fig. 10, give

$$2(F_2 + F_3) = 2 \times 27.18 = 54.3 \text{ lbf}$$

$$F_1 = (P_i - P_0)A_i + m_i V_i = 17.5 \text{ lbf}$$

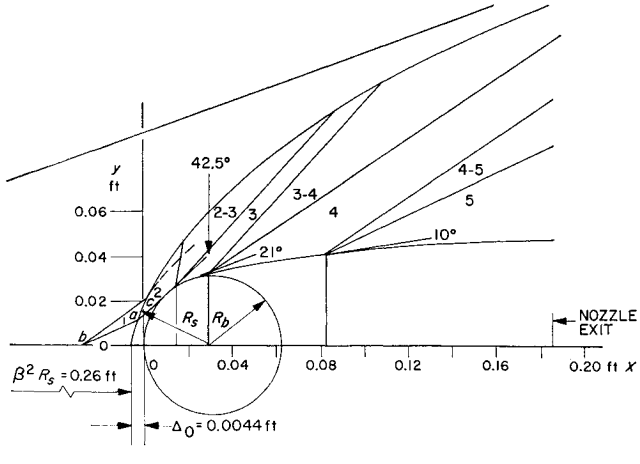

Fig. 10 Sample calculation of side force for case 2 of numerical example.

$$F_t = 54.3 + 17.5 = 71.8 \text{ lbf}$$

$$F_t \cos 17.5° = 68 \text{ lbf}$$

The measured side force of case 2 was 56 lb.

Conclusions

In developing the analytical model, many assumptions were made which need further verification. Nevertheless, it is believed that the approach taken in this paper offers a useful and valid method for the calculation of side force generated by secondary liquid injection with a nonflashing liquid. The formulated model for flow interference is in agreement with the observed shock patterns. In addition to the side-force calculation from the analytical model, one can obtain the static pressure distribution along the nozzle wall.

The formulated model is based on a step-by-step approach, in which it is possible to improve an individual step based on experimental work without affecting the over-all construction of the model. For a complete understanding of the problem, further research is required in the following areas: 1) effects of mixing between the primary and secondary stream, 2) boundary-layer thickness, 3) jet penetration, and 4) liquid atomization in supersonic flow.

The model can be used to optimize injector and mainstream conditions for the generation of maximum side force for a given set of conditions. However, such parametric studies were not undertaken in this program. The numerical process may appear tedious, but solutions to many of the steps can be facilitated by digital computations.

References

[1] Hozaki, S., Mayer, E., and Rao, G. V. R., "Thrust vector control by secondary injection into rocket exhaust," ARS Preprint 2656-62 (November 1962).

[2] Wu, J. M., Chapkis, R. L., and Mager, A., "An approximate analysis of thrust vector control by fluid injection," ARS J. 31, 1677–1685 (1961).

[3] Wu, J. M., Chapkis, R. L., Ai, D. K., and Rao, G. V. R., "Polaris thrust vector control analysis," National Engineering and Science Co. Final Rept. Contract P. O. S-412707-OP, Pasadena, Calif. (July 1961).

[4] Ingebo, R. and Foster, H., "Drop-size distribution for cross-current break-up of liquid in airstreams," NACA TN 4087 (October 1957).

[5] Longwell, J. P., "Combustion of liquid fuels," *High Speed Aerodynamics and Jet Propulsion* (Princeton University Press, Princeton, N. J., 1956), Vol. II, Sec. J, p. 412.

[6] Bitron, M. D., "Atomization of liquids by supersonic air jets," Ind. Eng. Chem. **47,** 23–28 (January 1955).

[7] Godsave, G. A. E., "Studies of combustion of drops in a fuel spray—the burning of single drops of fuel," *Fourth International Symposium on Combustion, 1952* (Williams and Wilkins Co., Baltimore, Md., 1952), pp. 818–830.

[8] Godsave, G. A. E., "Studies of combustion of drops in a fuel spray—the burning of single drops of fuel" (see discussion by J. A. Bierlein and K. Scheller), *Fourth International Symposium on Combustion, 1952* (Williams and Wilkins Co., Baltimore, Md., 1952), pp. 829–830

[9] Agoston, G. A., Wise, H., and Rosser, W. A., "Dynamic factors affecting the combustion of liquid spheres," *Sixth International Symposium on Combustion, 1956* (Reinhold Publishing Co., New York, 1956), pp. 708–717.

[10] Stansel, J., "Literature search of drag and heat transfer coefficients of spherical particles," Jet Propulsion Lab., Pasadena, Calif. (unpublished).

[11] Perry, J. H., *Chemical Engineer's Handbook* (McGraw-Hill Book Company, New York, 1950), 3rd ed., pp. 1017–1020.

[12] Stonecypher, T. E., *Dynamic and thermal non-equilibrium in two-phase flow in rocket nozzles,"* Rohm and Haas Co., Quarterly Progress Rept. P-60-17, Huntsville, Ala. (September 1960).

[13] Mayer, E., Houser, B., and Hays, W., "Feasibility studies of adverse pressure gradient nozzles for liquid injectant thrust vector control," National Engineering Science Co. Final Rept. to LMSC, Subcontract 18-10468, Pasadena, Calif., Vol. 1 (November 1962).

[14] Dowdy, M. W. and Newton, J. F., "Wind tunnel experiments on Freon-12 secondary injection," *Space Program Summary no. 37-17* (Jet Propulsion Lab., Pasadena, Calif., October 1962), Vol. IV.

[15] Hayes, W. D. and Probstein, R. F., *Hypersonic Flow Theory* (Academic Press, Inc., New York, 1959), pp. 139–165.

[16] Mager, A., "On the model of the free, shock-separated, turbulent boundary layer," J. Aeronaut. Sci. **23,** 181–186 (1956).

[17] Hozaki, S., Mayer, E., Tromblay, J., and Wu, J., "Investigation of boundary layer parameters in APG nozzle and the flow interference by secondary injection," National Engineering Science Co. Final Rept., NASA Contract Nas7-177, Pasadena, Calif. (March 1963).

[18] Thompson, T. and Hoffman, H., "Oblique shock charts," Space Technology Lab. Rept. GM-TN-0165-00-201, Los Angeles (November 24, 1958).

[19] Sehgal, R. and Wu, J. M., "A study of thrust vector control by liquid injection into rocket nozzles," TM 33-138, Jet Propulsion Lab., Pasadena, Calif. (May 1, 1963).